Note S1: Derivation of species-specific morphological traits

Tree height (H, m) and crown diameter (D_{crown}, m) of individual trees were constrained in the mangrove growth model using the field data-derived species-specific morphological traits. The H of individuals usually obeys allometric scaling relationship expressed as

$$H = \beta_{\mathrm{H}}\mathrm{DBH}^{\alpha} \quad \text{(S1)}$$

where β_{H} is the normalization term, α is the scaling exponent, and DBH is the diameter at breast height (m) (West et al., 2009). However, mangroves probably show some flexibility in the DBH-H relationship depending on environmental variables such as soil salinity (Peters et al., 2014). Figure S1a–b shows the compilation of DBH-H data from Fukido mangrove forest for the two species, and indeed the data showed some variabilities of H relative to DBH especially for relatively large trees (DBH > 0.1 m). To allow flexibility in the DBH-H relationship but to constrain it within the observed range, we derived two allometric relationships for H – DBH-maximum tree height (H_{max}) and DBH-minimum tree height (H_{min}) relationships – as follows. We first binned H data with the DBH width of 0.01 m for *Rhizophora stylosa* and 0.02 m for *Bruguiera gymnorrhiza*, where the choice of different binning widths was attributed to the different data densities in bins between the two species. Maximum and minimum H were then extracted for each bin, and were fitted to Eq. (S1) to obtain DBH-H_{max} and DBH-H_{min} relationships, respectively. Here, we removed from the fitting some binned data that could be outliers to avoid under- or overestimation of H_{max} and H_{min}. Additionally, we derived the general allometric relationship of DBH-H for each species by fitting all the data to Eq. (S1). This relationship was used to estimate H of trees whose H was not measured in the field as described in the Section 2.2. The fitted curves are shown in Fig. S1a–b.

The parameter D_{crown} also usually follows an allometric scaling relationship, where the scaling exponent is often assumed to be 2/3 based on a metabolic scaling theory (West et al., 2009; Shenkin et al., 2020):

$$D_{\mathrm{crown}} = \beta_{\mathrm{crown}} \mathrm{DBH}^{2/3} \quad \text{(S2)}$$

where β_{crown} is the normalization term for crown diameters. However, crown structures are significantly influenced by tree competition, resulting in variability of D_{crown} (Pretsch, 2014; Jucker et al., 2015). Here, we assumed that the crown diameter of the allometric ideal trees (D^*_{crown}) follows Eq. (S2), where we refer to allometric ideal as the condition where the crown expansion is not influenced by local competition. We derived the coefficient β_{crown} of D^*_{crown} for the two species using a similar approach of deriving DBH-H_{max} relationships. For *B. gymnorrhiza*, the data of D_{crown} were binned with DBH width of 0.02 m, and the maxima in bins of DBH < 0.1 m were extracted. The maxima were assumed to represent D^*_{crown} and were fitted to Eq. (S2) to derive β_{crown} (Fig. S1d). We removed the maxima of DBH > 0.1 m from fitting because of less certainty in the representation of D^*_{crown} for large trees due to data scarcity compared to smaller trees. Alternatively, D_{crown} of *R. stylosa* showed significantly different trend from *B. gymnorrhiza* – none of the measured D_{crown} exceeded 2.0 m, which implies the strong influence of local competition for this species. Therefore, we supplemented the data with D_{crown} from two different mangrove forests in the Philippines and Indonesia (see Note S2 for the details). Specifically, supplemented data for large trees (DBH > 0.1 m) were from relatively open canopy forests, thus it is more probable that the data represent D^*_{crown}. Note that the supplemented data used are from *R. apiculata* and *R. mucronata*, which are so far the only available data on the crown diameter of *Rhizophora* species, and may apply to *R. stylosa*. After combining the data from Fukido mangrove and other two sites, we binned the data with DBH width of 0.02 m, and the maxima were fitted to Eq. (S2) to estimate β_{crown} for *R. stylosa* (Fig. S1c); some maxima that could be outliers were removed from the fitting.

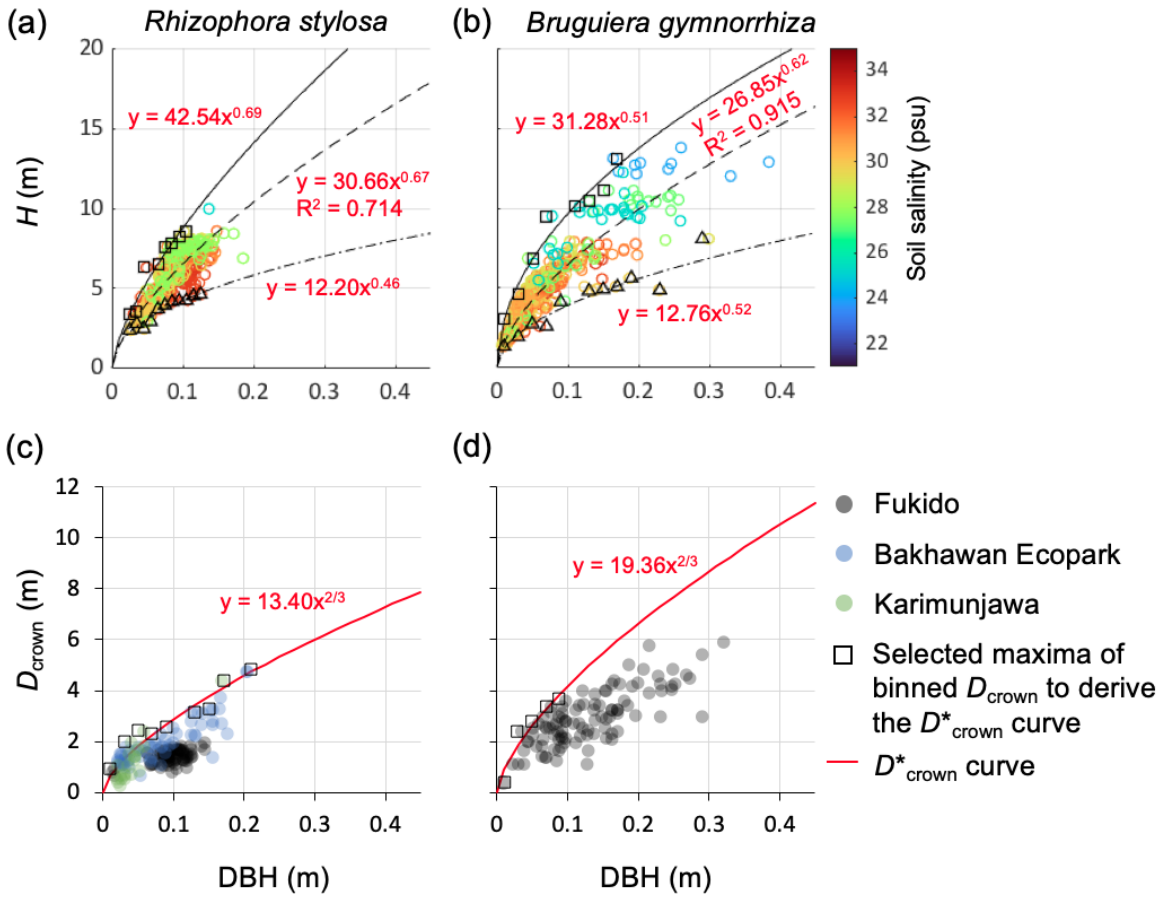

48

49 Fig. S1. Field data-derived morphological traits of *Rhizophora stylosa* and *Bruguiera*
50 *gymnorrhiza*. (a–b) DBH-tree height (H) relationships and (c–d) DBH-crown diameter (D_{crown})
51 relationships of the two species in Fukido mangrove forest. In panels (a–b), the solid and dot-
52 dash lines indicate DBH-maximum height (H_{max}) and DBH-minimum height (H_{min})
53 relationships, respectively, while the rectangular and triangular markers indicate the maxima
54 and minima of selected bins used for the derivation of DBH-H_{max} and DBH-H_{min} relationships,
55 respectively. The dashed lines indicate the general allometric relationship of DBH-H. In panel
56 (c), the supplemented data from *R. apiculata* and *R. mucronata* in Bakhawan Ecopark and
57 Karimunjawa, and *R. stylosa* in Fukido were used.

Note S2: Supplementary data on crown diameters

Supplementary measurements of crown diameter for the genus *Rhizophora* were conducted in a planted mangrove forest in Bakhawan Ecopark, Panay Island, Philippines and a dwarf mangrove forest in Karimunjawa Island, Central Java, Indonesia. In Bakhawan Ecopark, ~10- (11.7195°N, 122.3927°E), ~20- (11.7180°N, 122.3892°E), and ~30-year-old forests (11.7180°N, 122.3911°E) were selected so that the measurement will have a wide range in tree size variability. In each forest, 20 trees were randomly selected, and the crown diameters were measured using the same protocol as described in Section 2.2. The forests are mix of *R. apiculata* and *R. mucronata* stands, and sampled trees cover diameters at breast height (DBH) of ~0.05 m, 0.05–0.13 m, and 0.1–0.2 m at ~10-, ~20-, and ~30-year-old forests, respectively. Photographs of the canopy taken by looking upward are shown in Fig. S2a–c. The canopy of ~10- and ~20-year-old forests are closed while the canopy of ~30-year-old forest is relatively open. The mangrove forest in Karimunjawa Island is a mix of natural and planted stands of *R. apiculata* and *R. mucronata*. The canopy is completely open; thus, no influence of competition is expected (Fig. S2d). The sampled trees cover DBH of 0.02–0.17 m.

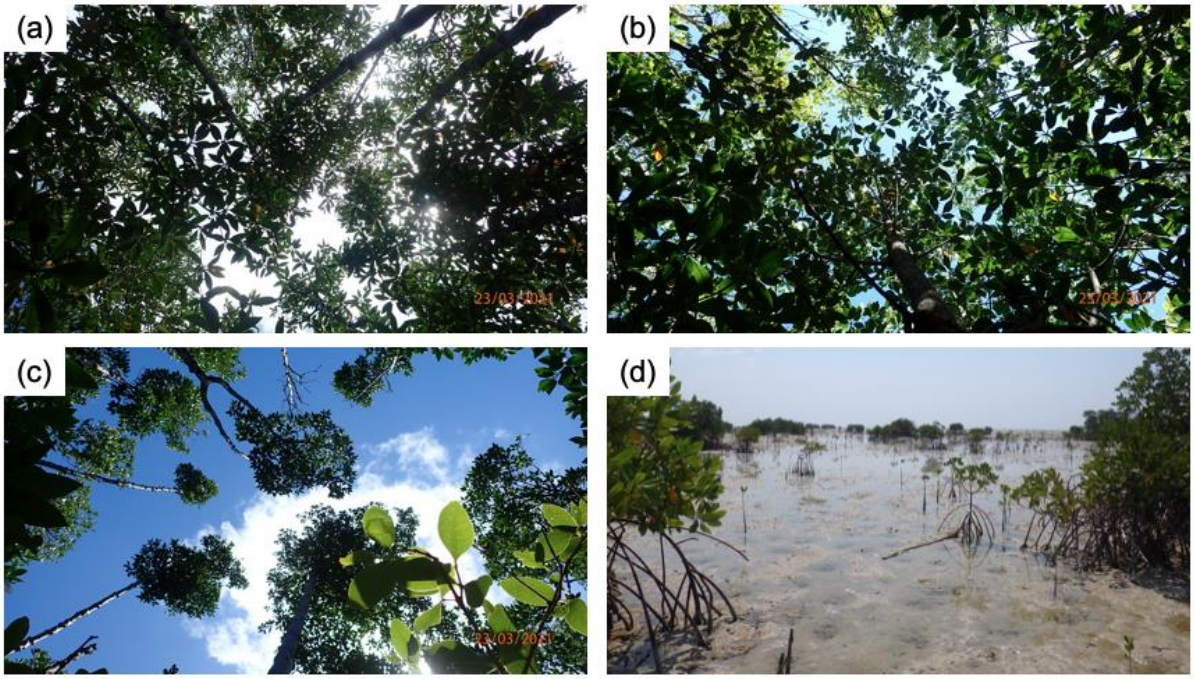

Fig. S2. Upward-looking view of canopies in (a) ~10-, (b) ~20-, and (c) ~30-year-old forests in Bakhawan Ecopark, and (d) view of a dwarf mangrove forest in Karimunjawa Island.

Note S3: Minor modification of processes in SEIB-DGVM

Tree establishment

The computational domain is divided into 1 m × 1 m grid-cells, and the establishment of a tree is simulated at each grid-cell at yearly time step according to establishment probability and some criteria. The original SEIB-DGVM defines criteria of climate conditions for the establishment to reproduce the global vegetation distribution (Sato et al., 2007). However, the site of model application in this study is small and the spatial variations in atmospheric variables are not expected, thus such criteria were not considered in this study. Therefore, the environmental factor that affects the establishment is only annual-mean midday photosynthetically active radiation at the forest floor in a grid-cell (PAR_{floor}). If $PAR_{floor} > PAR_{min}$, the grid-cell has the potential of new establishment of a species, where PAR_{min} is the minimum PAR_{floor} required to establish the species. If several species satisfied this condition, the species that will establish in the grid cell is determined according to the fraction of total biomass of each species in the computational domain such that the dominant species has a higher probability of establishment. Simultaneously, it is sometimes randomly selected with a probability Est_{random}, where the value of Est_{random} was set as 0.05 in this study. This corresponds to Scenario 4 in the tree establishment scheme in SEIB-DGVM (see Sato, 2015 for the detail). Then, the determined species establishes at the grid cell with a probability $P_{establish}$ (m^{-2} $year^{-1}$).

Mortality

Mortality occurs at a yearly time step in SEIB-DGVM. Mortality is usually modeled as a sum of growth efficiency mortality ($mort_{greff}$, $year^{-1}$) and background mortality ($mort_{bg}$, $year^{-1}$) in dynamic vegetation models. Additionally, SEIB-DGVM introduced heat stress- or cold stress-induced mortality to describe global vegetation distribution (Sato et al., 2007), but these

additional factors were not considered in this study for the same reason as the establishment. The SEIB-DGVM also defines the maximum age that trees can survive, but it was also not considered in this study due to the uncertainty in the longevity of mangroves. Also, the formulation of growth-efficient mortality was replaced with the following equation which is used as such in Sitch et al. (2003) and Thum et al. (2019):

$$mort_{\mathrm{greff}} = \frac{k1_{\mathrm{mort\_greff}}}{1+k2_{\mathrm{mort\_greff}} \times eff_{\mathrm{growth}}} \quad \text{(S3)}$$

where $k1_{\mathrm{mort\_greff}}$ (year^{-1}) and $k2_{\mathrm{mort\_greff}}$ (m^2 leaf year g^{-1} Dry Weight) are parameters and eff_{growth} (g DW m^{-2} leaf year^{-1}) is the net primary production minus tissue turnover per unit leaf area which is described as

$$eff_{\mathrm{growth}} = \frac{NPP-TO}{LA} \quad \text{(S4)}$$

where *NPP* is the annual net primary production (g DW tree^{-1} year^{-1}), *TO* is the annual whole-plant turnover demand (g DW tree^{-1} year^{-1}), and *LA* is the whole-plant leaf area (m^2 leaf tree^{-1}). The equation was replaced because the original equation in SEIB-DGVM has a parameter with a physically complicated unit.

In this study, we introduced additional mortality that is related to salt stress ($mort_{\mathrm{salt}}$, year^{-1}). As described in Section 2.3.2, if a tree is stressed by salt, the tree adjusts plant hydraulics from the sapwood area or root biomass (Eq. (7)). Consequentially, *H* of the tree could go below the DBH-H_{min} curve shown in Fig. S1a–b, depending on salt stress. In such a case, the tree was regarded as "salt-stressed tree" and high mortality was given. In this study, $mort_{\mathrm{salt}}$ was set to 0.3 for salt-stressed trees and 0.0 for non-stressed trees. Then, the mortality of a tree (f_{mort}, year^{-1}) is calculated by adding each mortality factor:

$$f_{\mathrm{mort}} = \min\left(mort_{\mathrm{greff}} + mort_{\mathrm{bg}} + mort_{\mathrm{salt}}, 1.0\right) \quad \text{(S5)}$$

Maintenance respiration

In SEIB-DGVM, a parameter called the specific respiration rate per unit nitrogen in the plant tissue at 15.0 ℃ (*RM*, g DW g^{-1} N day^{-1}) is used to calculate the maintenance respiration rate of each tree organ. However, for the leaf respiration, we used the dark respiration rate per unit area at 25 ℃ ($R_{d,25}$, μmol C m^{-2} s^{-1}) instead of *RM*, which is a common parameter for leaf respiration rate. For the temperature response of $R_{d,25}$, a function used in Kumarathunge et al. (2019) (also see Note S4) was used. For maintenance respiration of other organs, the parameters RM_W and RM_{FR} (respiration rate per unit biomass at 15.0 ℃, g DW g^{-1} DW day^{-1}) for woody organ and fine root, respectively, were used instead of *RM* to adopt literature values. Temperature response of maintenance respiration of these organs was kept the same as in the original SEIB-DGVM. Likewise, as in the original SEIB-DGVM, if the whole-plant gross primary production (g C $tree^{-1}$ day^{-1}) is insufficient for satisfying the whole-plant demand of maintenance respiration, the deficit is supplemented from the stock carbon pool.

Crown layer purge

In SEIB-DGVM, trees purge the bottom crown layer at yearly time step depending on the balance between resource gain and maintenance cost of the layer. Here, the resource gain of the layer is expressed using leaf-level net primary photosynthesis rate at the layer ($Crown_{C\_gain}$, g C m^{-2} leaf day^{-1}), while the maintenance cost ($Crown_{C\_cost}$, g C m^{-2} leaf day^{-1}) is expressed using:

$$Crown_{C\_cost} = \frac{TO_l \times C_M}{SLA \times 10^{-4}} \quad \text{(S6)}$$

where TO_l is the leaf turnover rate (day^{-1}), C_M is the carbon mass per unit dry weight in plant tissue (g C g^{-1} DW), SLA is the specific leaf area (cm^2 leaf g^{-1}), and the multiplication of 10^{-4} is for unit conversion of SLA.

In this study, nitrogen (N) uptake was also considered in addition to carbon uptake by photosynthesis, which emerges as an additional need for the consideration of gain and cost balance for N. The N uptake by a crown layer ($Crown_{\mathrm{N\_gain}}$, g N m^{-2} leaf day^{-1}) is expressed as:

$$Crown_{\mathrm{N\_gain}} = T_{\mathrm{layer}} \times \mathrm{DIN} \times \frac{14}{1000} \quad \text{(S7)}$$

where T_{layer} is the leaf-level transpiration rate at the bottom layer (T_{layer}, mm day^{-1}), DIN is the dissolved inorganic nitrogen concentration in porewater (mol N m^{-3}), and the multiplication of 14/1000 is for unit conversion. The N cost by the layer ($Crown_{\mathrm{N\_cost}}$, g N m^{-2} leaf day^{-1}) is expressed as:

$$Crown_{\mathrm{N\_cost}} = \frac{TO_{\mathrm{l}} \times \mathrm{C_M} \times (1 - NRE)}{\mathrm{SLA} \times \mathrm{CN_l}} \quad \text{(S8)}$$

where $\mathrm{CN_l}$ is the C/N ratio in the leaf (g C g^{-1} N), and *NRE* is the nitrogen resorption efficiency (fraction). A tree purges the crown layer if the annual mean of $Crown_{\mathrm{C\_gain}}$ or $Crown_{\mathrm{N\_gain}}$ is less than $Crown_{\mathrm{C\_cost}}$ or $Crown_{\mathrm{N\_cost}}$, respectively.

Note S4: Leaf flux model

Leaf temperature and transpiration

Leaf temperature and transpiration rates are calculated at each crown layer of each tree using the equations presented by Bonan et al. (2014); these are summarized below.

The leaf energy balance can be written by equating the net radiation ($R_{n,i}$, W m^{-2}) to the sum of sensible heat flux (H_i, W m^{-2}) and latent heat flux ($\lambda_w E_i$, W m^{-2}) at each crown layer, where the symbol "i" indicates crown layer index here and hereafter:

$$R_{n,i} = H_i + \lambda_w E_i \quad \text{(S9)}$$

where λ_w (J mol^{-1}) is the latent heat of vaporization of water and E_i is leaf transpiration rate at crown layer i (mol m^{-2} s^{-1}). The sensible heat flux H_i is represented as:

$$H_i = 2c_p(T_{l,i} - T_a)g_{bh,i} \quad \text{(S10)}$$

where c_p is the specific heat of air at constant pressure (J mol^{-1} K^{-1}), $T_{l,i}$ is the leaf temperature (K), T_a is the air temperature (K), and $g_{bh,i}$ is the boundary layer conductance for heat (mol m^{-2} s^{-1}). The parameter $g_{bh,i}$ is a function of leaf size (d_l, m) and wind speed. Here, wind speed profile within the canopy is calculated from a model proposed by Barnard and Bauerle (2016) by approximating a horizontally uniform canopy structure. Latent heat flux is given by:

$$\lambda_w E_i = \frac{c_p}{\gamma}(e_{l,i} - e_a)g_{v,i} \quad \text{(S11)}$$

where γ is the psychrometric constant (Pa K^{-1}) given by $\gamma = c_p P_a/\lambda_w$ with P_a atmospheric pressure (Pa), $e_{l,i}$ the leaf vapor pressure (Pa), e_a the air vapor pressure (Pa), and $g_{v,i}$ the conductance for water vapor (mol m^{-2} s^{-1}) expressed as a series of stomatal conductance ($g_{s,i}$, mol m^{-2} s^{-1}) and boundary layer conductance ($g_{bv,i}$, mol m^{-2} s^{-1}) with $g_{vi} = 1/(g_{s,i}^{-1} + g_{bv,i}^{-1})$. The parameter $g_{bv,i}$ is a function of leaf size and wind speed, similar to $g_{bh,i}$. It is assumed that the water vapor pressure in the stomatal pore is saturated; therefore $e_{l,i}$ is a function of leaf

179 temperature $T_{l,i}$. Here, once the value of $g_{s,i}$ is given, the values of $T_{l,i}$ and $E_{l,i}$ were determined
180 from Eqs. (S9)–(S11).

181 *Leaf photosynthesis*

182 Leaf photosynthesis is calculated using the biochemical model of Farquhar et al. (1980),
183 which was adapted by the leaf flux model of Bonan et al. (2011) and (2014). The equations are
184 summarized below.

185 The net leaf photosynthesis rate at a crown layer i ($A_{n,i}$, μmol CO_2 m^{-2} s^{-1}) is given by:

186 $$A_{\mathrm{n,i}} = \min\left(A_{\mathrm{c,i}} - A_{\mathrm{j,i}}\right) - R_{\mathrm{d}} \quad \text{(S12)}$$

187 $$A_{\mathrm{c,i}} = \frac{V_{\mathrm{cmax}}\left(c_{i,\mathrm{i}} - \Gamma_*\right)}{c_{i,\mathrm{i}} + K_{\mathrm{c}}\left(1 + o_i/K_{\mathrm{o}}\right)} \quad \text{(S13)}$$

188 $$A_{\mathrm{j,i}} = \frac{J_{\mathrm{i}}\left(c_{i,\mathrm{i}} - \Gamma_*\right)}{4c_{i,\mathrm{i}} + 8\Gamma_*} \quad \text{(S14)}$$

189 where $A_{c,i}$ and $A_{j,i}$ (μmol m^{-2} s^{-1}) are the Rubisco carboxylation-limited and RuBP-regeneration-
190 limited photosynthetic rates, respectively, R_d is the leaf respiration rate (μmol m^{-2} s^{-1}), $c_{i,i}$ is the
191 intercellular CO_2 concentration (μmol mol^{-1}), Γ_* is the CO_2 compensation point (μmol mol^{-1}),
192 V_{cmax} is the maximum rate of Rubisco activity (μmol m^{-2} s^{-1}), o_i is the intercellular O_2
193 concentration (209 mmol mol^{-1}), K_c (μmol mol^{-1}) and K_o (mmol mol^{-1}) are the Michaelis-
194 Menten coefficients of Rubisco activity for CO_2 and O_2 respectively, and J_i is the electron
195 transport rate at a crown layer i (μmol m^{-2} s^{-1}), which is related to absorbed PAR at the layer
196 ($APAR_i$, μmol photon m^{-2} s^{-1}); these are described as:

197 $$\theta_{PSII} J_{\mathrm{i}}^2 - \left(I_{PSII} + J_{\mathrm{max}}\right) J_{\mathrm{i}} + I_{PSII} J_{\mathrm{max}} = 0 \quad \text{(S15)}$$

198 $$I_{PSII} = 0.5(1 - f)\mathrm{APAR_i} \quad \text{(S16)}$$

199 where θ_{PSII} is the curvature for electron transport (0.7), I_{PSII} is the PAR absorbed by PS II (μmol
200 photon m^{-2} s^{-1}), f is a fraction of PAR absorbed by non-photosynthetic materials (0.15), and
201 J_{max} is the maximum electron transport rate (μmol m^{-2} s^{-1}). In Eqs. (S12)–(S15), the parameters

V_{cmax}, J_{max}, R_d, Γ_*, K_c, and K_o vary with leaf temperature, thus the values may vary within crown layers. Following Kumarathunge et al. (2019), the values and temperature responses of Γ_*, K_c, and K_o were adapted from Bernacchi et al. (2001) and Medlyn et al. (2002), respectively. The temperature response of V_{cmax} and J_{max} are given by the peaked Arrhenius function:

$$k_1(T_v) = k_{25} \times \exp\left[\frac{E_a(T_v - 298.15)}{298.15RT_v}\right] \frac{1+\exp\left(\frac{298.15\Delta S - H_d}{298.15R}\right)}{1+\exp\left(\frac{T_v\Delta S - H_d}{T_vR}\right)} \quad \text{(S17)}$$

while the temperature response of R_d is given by:

$$k_2(T_v) = k_{25} \times \exp\left[\frac{E_a(T_v - 298.15)}{298.15RT_v}\right] \quad \text{(S18)}$$

where $k_1(T_v)$ and $k_2(T_v)$ are the process rates at a given temperature, T_v (K), k_{25} is the process rate at 25 °C, R is the universal gas constant (J K^{-1} mol^{-1}), E_a is the activation energy (J mol^{-1}), H_d is the deactivation energy (J mol^{-1}), and ΔS is the entropy term (J K^{-1} mol^{-1}).

Gas exchange is regulated by the diffusion process between the atmosphere and the leaf through the stomata. The net photosynthesis rate $A_{n,i}$ can also be expressed using the diffusive rate given by:

$$A_{n,i} = \frac{(c_a - c_{i,i})}{1.4g_{bv,i}^{-1} + 1.6g_{s,i}^{-1}} \quad \text{(S19)}$$

where c_a is the atmospheric CO_2 concentration (μmol mol^{-1}), $c_{i,i}$ is the intercellular CO_2 concentration (μmol mol^{-1}), $g_{s,i}$ and $g_{bv,i}$ are the stomatal conductance and boundary layer conductance for water vapor (mol m^{-2} s^{-1}), respectively, and the factor 1.4 and 1.6 are for adjusting the diffusivity of CO_2 compared with H_2O for the boundary layer and stomatal conductance (Bonan, 2019). The value of $A_{n,i}$ can then be obtained once the value of $g_{s,i}$ is given by equating Eqs. (S12) and (S19).

Stomatal conductance optimization

The leaf transpiration rate, temperature, and photosynthetic rate at a crown layer depend on stomatal conductance at the layer. Here, the stomatal conductance at a layer, $g_{s,i}$, is estimated from the optimization theory. The theory assumes that plants regulate stomatal conductance to keep the marginal water use efficiency (WUE) constant (Cowan and Farquhar, 1977), which has been used in the models of Bonan et al. (2014) and Xu et al. (2016). The stomatal conductance is optimized at each crown layer to achieve the condition:

$$\frac{\mathrm{d}A_{\mathrm{n,i}}}{\mathrm{d}g_{\mathrm{s,i}}} - \lambda \frac{\mathrm{d}E_{\mathrm{i}}}{\mathrm{d}g_{\mathrm{s,i}}} = 0 \quad \text{(S20)}$$

where λ is the Lagrangian multiplier of the optimization problem representing optimal WUE. This is a condition that indicates that the further opening of stomata does not yield a sufficient carbon gain per unit water loss, characterized by λ (Bonan et al., 2014). We followed Bonan et al. (2014) for the numerical solution of $g_{s,i}$. The value of λ increases as leaf water potential (Ψ_l, MPa) declines, as shown by a meta-analysis of Manzoni et al. (2011), where the increased λ generally leads to the regulation of stomatal conductance, resulting in decreased A_n and E. Then, following Xu et al. (2016), λ is determined at daily time step considering predawn leaf water potential ($\Psi_{l,predawn}$, MPa):

$$\lambda = \lambda_0 \exp\left(\beta_0 \Psi_{\mathrm{l,predawn}}\right) \quad \text{(S21)}$$

where λ_0 is the value of optimal WUE when there is no stress imposed by the decreased leaf water potential, and β_0 is an empirical parameter representing stomatal sensitivity. Additionally, when Ψ_l falls below a species-specific minimum value given by $\Psi_{l,min}$, the model simulates stomatal closure to prevent further decrease in Ψ_l that may cause xylem cavitation (Bonan et al., 2014).

Note S5: Daily C and N resources for tree growth

From the plant hydraulics module coupled with the photosynthesis module described in the section 2.3.1 and Note S4, the daily C (C_{gain}, g C tree^{-1} day^{-1}) and N (N_{gain}, g N tree^{-1} day^{-1}) uptake rates were calculated, where N_{gain} is given by:

$$N_{gain} = J_{sap,day} \times DIN \times \frac{14}{\rho_w} \approx T_{whole,day} \times DIN \times \frac{14}{\rho_w} \quad (S22)$$

where, $J_{sap,day}$ and $T_{whole,day}$ are the daily sap flow and whole-plant transpiration rates (kg tree^{-1} day^{-1}), DIN is the dissolved inorganic nitrogen concentration in the porewater (mol N m^{-3}), ρ_w is water density (kg m^{-3}), and the factor 14 is for unit conversion of N from molar to gram concentration. Although the sap flow and whole-plant transpiration rates may differ at a short time step (e.g., hourly), these are equivalent at relatively a long time scale (e.g., daily); therefore, $J_{sap,day} \approx T_{whole,day}$. The C_{grow} (daily C resources that can be used for tree growth, g C tree^{-1} day^{-1}) was calculated from C_{gain} using the following steps: subtraction for the whole-plant woody and root maintenance respiration and C cost for turnover compensation after accounting for growth respiration, and subtraction/addition of C deficit/surplus in the stock pool from the target value characterized by a parameter β_{stock} (Table 1). Likewise, N_{grow} (daily N resources that can be used for tree growth, g N tree^{-1} day^{-1}) was calculated from N_{gain} by subtraction of N cost for turnover compensation, the addition of N resorbed from the senescent leaves characterized by a parameter *NRE* (Table 1), and subtraction/addition of N deficit/surplus in the stock pool from the target value. Suppose C_{gain} or N_{gain} is insufficient for compensating the respiration (only for C_{gain}) and turnover cost, the deficit is supplemented from the stock pool, where the growth respiration is accounted for in the case of C compensation for the turnover cost.

Note S6: Crown diameter expansion

When biomass is allocated to leaves in a tree, the model simulates the increase of crown area or leaf area index (LAI) of the tree, depending on the crown morphology at a specific time. We considered that plants preferentially increase crown area rather than LAI to increases their occupied space if the expansion of crown diameter (D_{crown}) is not inhibited by allometric (D^*_{crown}) or physical ($D_{crown.con}$) constraints. The crown diameter expansion is also beneficial in terms of plant productivity because the increase in LAI attenuates radiation within the crown more rapidly, decreasing the photosynthetic and transpiration rates per unit leaf area.

If an increase in leaf biomass is given by dM_L (g leaf tree^{-1} day^{-1}) and the crown diameter expansion is not inhibited ($D_{crown} < \min(D^*_{crown}, D_{crown,con})$), the tree expands its crown by keeping the same LAI as follows:

$$\frac{M_L}{A_{crown}} = \frac{M_L + dM_L}{A_{crown} + dA_{crown}} \quad \text{(S23)}$$

where A_{crown} is the crown area, and dA_{crown} is the increase in crown area due to crown diameter expansion. Crown diameter after the expansion is then calculated from the value (A_{crown} + dA_{crown}).

Table S1. Summary of environmental and vegetation variables at survey plots. AGB = above-ground biomass, DBH = diameter at breast height, *R.s* = *Rhizophora stylosa*, *B.g* = *Bruguiera gymnorrhiza*. The names of transects are indicated as A–D while plots along a transect line are numbered from the nearest creek to landward (Fig. 1c).

Plot	Soil salinity (psu)	Porewater NH_4^+ (μmol L^{-1})	Porewater NO_3^- (μmol L^{-1})	Porewater DIN (μmol L^{-1})	AGB (Mg ha^{-1}), *R.s*	AGB (Mg ha^{-1}), *B.g*	Mean DBH (m), *R.s*	Mean DBH (m), *B.g*
A1	32.8	190	21	212	92	1	9.1	6.1
A2	32.53	219	31	250	87	23	9.9	9.5
A3	33.0	238	22	260	63	30	9.1	7.3
A4	29.7	49	5	54	69	38	8.3	8.4
A5	29.9	69	8	76	10	19	6.2	10.7
B1	31.2	154	5	159	71	39	9.9	9.5
B2	31.7	272	7	279	87	26	10.4	9.1
B3	29.3	293	8	302	94	29	9.8	9.7
B4	27.8	124	4	129	108	19	10.3	12.2
B5	27.2	83	4	87	0	127	-	17.0
B6	24.1	98	9	107	0	144	-	23.9
B7	25.3	119	26	145	4	110	13.7	14.2
C1	29.3	115	6	121	0	180	-	16.5
C2	30.0	143	11	154	0	124	-	14.4
C3	24.5	186	20	206	16	120	12.8	15.0
C4	27.6	242	29	272	0	143	-	15.2
C5	31.7	262	20	283	11	143	12.3	10.5
D1	28.7	233	15	249	16	122	12.2	11.4
D2	30.7	247	18	265	12	114	9.5	13.4
D3	29.0	290	20	311	40	59	9.3	8.6
D4	26.2	181	9	190	0	185	-	19.3
D5	19.0	183	8	191	0	197	-	19.4
D6	22.2	167	11	178	0	152	-	20.6
D7	20.8	312	19	332	0	184	-	16.9

Table S2. Summary of model parameters not shown in Table 2.

Symbol	Description	Units	R. s	B. g	Source
C_M	Carbon mass per unit dry weight in plant tissue	g C g^{-1} DW	0.45	0.45	Alongi (2003)
a_1	Correction factor for tree height to water path length	–	1.2	1.2	Xu et al. (2016)
C_M	Carbon mass per unit dry weight in plant tissue	g C g^{-1} DW	0.45	0.45	Alongi et al. (2003)
F_{gr}	Growth respiration fraction	Fraction	0.25	0.25	Arora (2002)
PAR_{min}	Minimum PAR_{floor} required for establishment	μmol photon m^{-2} s^{-1}	100	100	
$P_{establish}$	Establishment probability	m^{-2} $year^{-1}$	0.1	0.1	
k_{1mort_greff}	Mortality parameter in Eq. (S3)	$year^{-1}$	0.1	0.1	
k_{2mort_greff}	Mortality parameter in Eq. (S3)	m^2 leaf year g^{-1} DW	0.03	0.03	
$mort_{bg}$	Background mortality rate	$year^{-1}$	0.07	0.07	Fisher et al. (2010)
RM_W	Maintenance respiration rate of woody organ at 15 ℃	g DW g^{-1} DW day^{-1}	6.5×10^{-5}	6.5×10^{-5}	Vinh et al. (2019)
RM_{FR}	Maintenance respiration rate of fine root at 15 ℃	g DW g^{-1} DW day^{-1}	4.3×10^{-3}	4.3×10^{-3}	Lovelock et al. (2006)
$R_{d,25}$	Dark leaf respiration rate at 25 ℃	μmol C m^{-2} s^{-1}	1.2	1.2	Aspinwall et al. (2021)
$J_{max,25}$	Maximum electron transport rate at 25 ℃	μmol C m^{-2} s^{-1}	1.54 × $V_{cmax,25}$		Aspinwall et al. (2021)
E_{aV}	Activation energy of the maximum rate of Rubisco activity (V_{cmax})	J mol^{-1}	108200	108200	Aspinwall et al. (2021)
E_{aJ}	Activation energy of the maximum electron transport rate (J_{cmax})	J mol^{-1}	73100	73100	Aspinwall et al. (2021)
E_{aR}	Activation energy of the dark leaf respiration rate (R_d)	J mol^{-1}	46400	46400	Bonan et al. (2014)
H_{dV}	Deactivation energy of V_{cmax}	J mol^{-1}	200000	200000	Kumarathunge et al. (2019)
H_{dJ}	Deactivation energy of J_{cmax}	J mol^{-1}	200000	200000	Kumarathunge et al. (2019)
ΔS_V	Entropy of V_{cmax}	J K^{-1} mol^{-1}	655	655	Aspinwall et al. (2021)
ΔS_J	Entropy of J_{cmax}	J K^{-1} mol^{-1}	655	655	Aspinwall et al. (2021)
d_l	Leaf dimension	m	0.1	0.1	

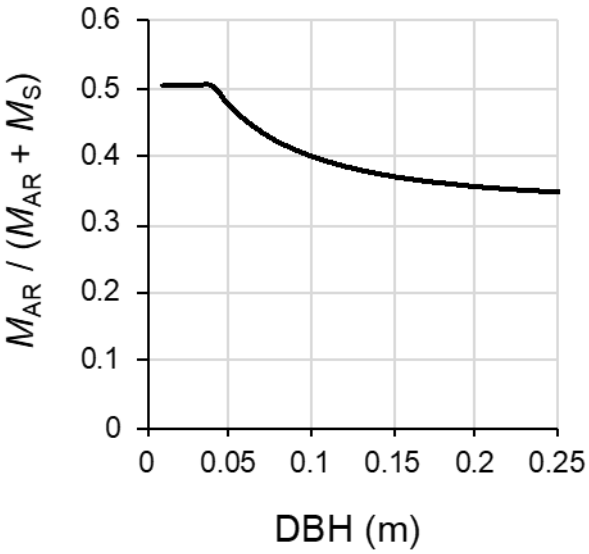

289

290 Fig. S3. Example of prop root allometry in Fukido mangrove forest. The parameter M_{AR} is
291 above-ground root (prop root) biomass, and M_S is stem biomass. The parameter M_S was
292 calculated from the diameter at breast height (DBH), tree height (H), and wood density (ρ)
293 using Eq. (1); H was calculated from the general allometric relationship shown in Fig. S1a. The
294 prop root biomass was calculated by multiplying the prop root volume and ρ; the prop root
295 volume was estimated from DBH and prop root diameter using the empirical model developed
296 for Fukido mangrove forest in Yoshikai et al. (2021). Here, the prop root diameter was set as
297 0.03 m based on field data. For trees with DBH < 0.03 m, the value computed for the tree with
298 DBH = 0.03 m was applied. Note that H does not always follow the general allometric
299 relationship in the simulation, therefore the prop root biomass fraction may vary from the one
300 shown here.

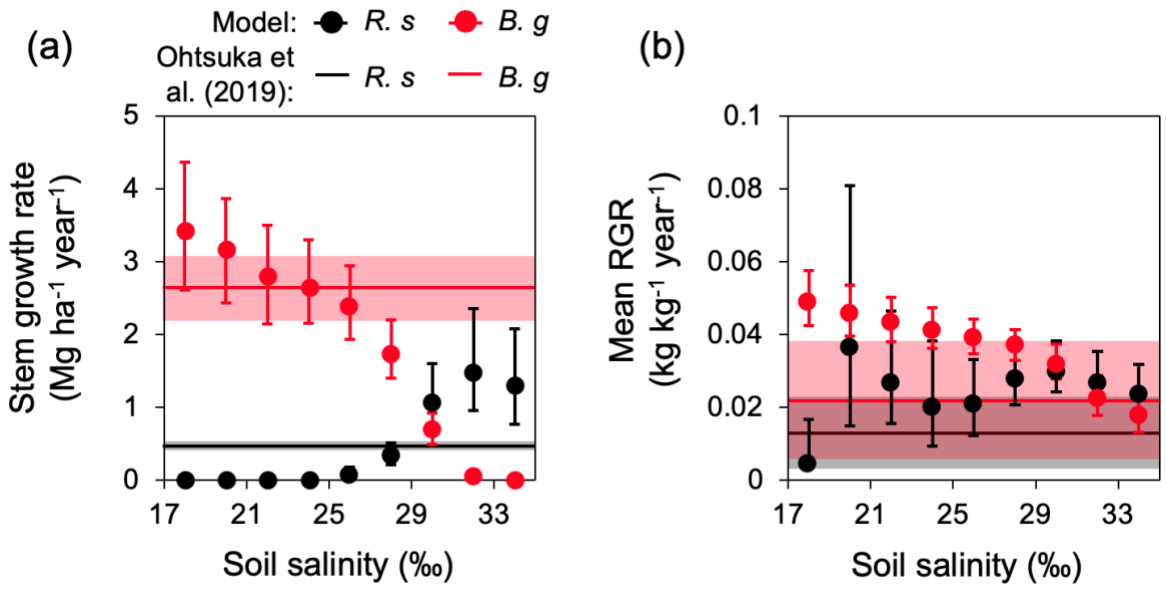

301

302 Fig. S4. (a) Stem growth rate and (b) mean individual relative growth rate (RGR) of *R. stylosa*
303 (*R. s*) and *B. gymnorrhiza* (*B. g*) along the soil salinity gradient. From each ensemble simulation,
304 the modeled stem growth rate and mean RGR in steady states (> 300 years) were extracted and
305 pooled for all ensembles, and the mean (circle marker) and standard deviation (error bar) values
306 of the pooled samples were shown. The line and shade show the mean and standard deviation
307 of data measured by Ohtsuka et al. (2019) in a *B. gymnorrhiza*-dominated site in Fukido
308 mangrove forest.

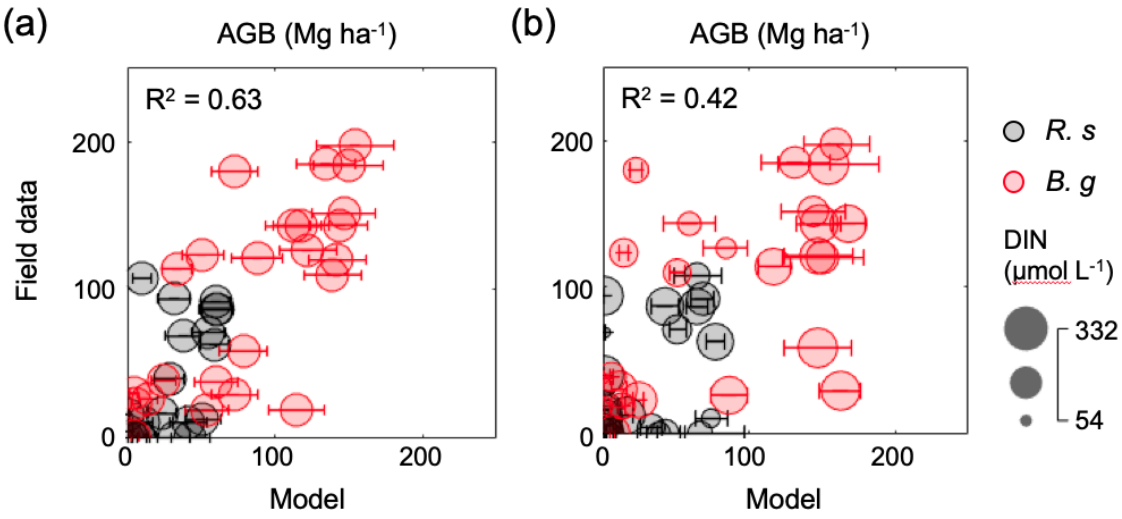

309

310 Fig. S5. Results of "plot-wise simulation". Comparison of modeled and field-measured AGB
311 at survey plots in Fukido mangrove forest, where panel (a) is a case where spatially averaged
312 DIN (200 μmol L^{-1}) was given while panel (b) is a case where plot-wise DIN is given. The
313 results shown are from one simulation, where modeled AGB in steady states (> 300 years) was
314 extracted and the median (circles) and the 90-th percentile (bars) were shown.

References

Alongi, D. M., Clough, B. F., Dixon, P., & Tirendi, F. (2003). Nutrient partitioning and storage in arid-zone forests of the mangroves *Rhizophora stylosa* and *Avicennia marina*. Trees, 17(1), 51–60.

Arora, V. (2002). Modeling vegetation as a dynamic component in soil‐vegetation‐atmosphere transfer schemes and hydrological models. Reviews of Geophysics, 40(2), 3–1.

Aspinwall, M. J., Faciane, M., Harris, K., O'Toole, M., Neece, A., Jerome, V., ... & Feller, I. C. (2021). Salinity has little effect on photosynthetic and respiratory responses to seasonal temperature changes in black mangrove (*Avicennia germinans*) seedlings. Tree Physiology, 41(1), 103–118.

Barnard, D. M., & Bauerle, W. L. (2016). Seasonal variation in canopy aerodynamics and the sensitivity of transpiration estimates to wind velocity in broadleaved deciduous species. Journal of Hydrometeorology, 17(12), 3029–3043.

Bernacchi CJ, Singsaas EL, Pimentel C, Portis AR Jr, Long SP. (2001). Improved temperature response functions for models of Rubisco-limited photosynthesis. Plant, Cell & Environment 24: 253–259.

Bonan, G. B. (2019). Climate change and terrestrial ecosystem modeling. Cambridge, UK; New York, NY: Cambridge University Press.

Bonan, G. B., Lawrence, P. J., Oleson, K. W., Levis, S., Jung, M., Reichstein, M., ... & Swenson, S. C. (2011). Improving canopy processes in the Community Land Model version 4 (CLM4) using global flux fields empirically inferred from FLUXNET data. Journal of Geophysical Research: Biogeosciences, 116(G2).

Bonan, G. B., Williams, M., Fisher, R. A., & Oleson, K. W. (2014). Modeling stomatal conductance in the earth system: linking leaf water-use efficiency and water transport along the soil–plant–atmosphere continuum. Geoscientific Model Development, 7(5), 2193–2222.

Cowan, I. R. and Farquhar, G. D.: Stomatal function in relation to leaf metabolism and environment, in: Integration of Activity in the Higher Plant, edited by: Jennings, D. H., Cambridge University Press, Cambridge, 471–505, 1977.

Fisher, R., McDowell, N., Purves, D., Moorcroft, P., Sitch, S., Cox, P., ... & Ian Woodward, F. (2010). Assessing uncertainties in a second‐generation dynamic vegetation model caused by ecological scale limitations. New Phytologist, 187(3), 666–681.

Jucker, T., Bouriaud, O., & Coomes, D. A. (2015). Crown plasticity enables trees to optimize canopy packing in mixed‐species forests. Functional Ecology, 29(8), 1078–1086.

Kumarathunge, D. P., Medlyn, B. E., Drake, J. E., Tjoelker, M. G., Aspinwall, M. J., Battaglia, M., ... & Way, D.A. (2019). Acclimation and adaptation components of the temperature dependence of plant photosynthesis at the global scale. New Phytol, 222: 768–784.

Lovelock, C. E., Ruess, R. W., & Feller, I. C. (2006). Fine root respiration in the mangrove *Rhizophora mangle* over variation in forest stature and nutrient availability. Tree physiology, 26(12), 1601–1606.

Manzoni, S., Vico, G., Katul, G., Fay, P. A., Polley, W., Palmroth, S., & Porporato, A. (2011). Optimizing stomatal conductance for maximum carbon gain under water stress: a

meta‐analysis across plant functional types and climates. Functional Ecology, 25(3), 456–467.
Medlyn, B. E., Dreyer, E., Ellsworth, D., Forstreuter, M., Harley, P. C., Kirschbaum, M. U. F., ... & Loustau, D. (2002). Temperature response of parameters of a biochemically based model of photosynthesis. II. A review of experimental data. Plant, Cell & Environment, 25(9), 1167–1179.
Ohtsuka, T., Tomotsune, M., Suchewaboripont, V., Iimura, Y., Kida, M., Yoshitake, S., ... & Kinjo, K. (2019). Stand dynamics and aboveground net primary productivity of a mature subtropical mangrove forest on Ishigaki Island, south-western Japan. Regional Studies in Marine Science, 27, 100516.
Peters, R., Vovides, A. G., Luna, S., Grüters, U., & Berger, U. (2014). Changes in allometric relations of mangrove trees due to resource availability–A new mechanistic modelling approach. Ecological Modelling, 283, 53–61.
Pretzsch, H. (2014). Canopy space filling and tree crown morphology in mixed-species stands compared with monocultures. Forest Ecology and Management, 327, 251–264.
Sato, H. (2015). SEIB-DGVM v2.80 online description document (http://seib-dgvm.com).
Sato, H., Itoh, A., & Kohyama, T. (2007). SEIB–DGVM: A new Dynamic Global Vegetation Model using a spatially explicit individual-based approach. Ecological Modelling, 200(3–4), 279–307.
Shenkin, A., Bentley, L. P., Oliveras, I., Salinas, N., Adu-Bredu, S., Marimon-Junior, B. H., ... & Malhi, Y. (2020). The influence of ecosystem and phylogeny on tropical tree crown size and shape. Frontiers in Forests and Global Change, 3, 109.
Sitch, S., Smith, B., Prentice, I. C., Arneth, A., Bondeau, A., Cramer, W., Kaplan, J. O., … & Venevsky, S. (2003). Evaluation of ecosystem dynamics, plant geography and terrestrial carbon cycling in the LPJ dynamic global vegetation model. Global Change Biology, 9: 161–185. https://doi.org/10.1046/j.1365-2486.2003.00569.x
Thum, T., Caldararu, S., Engel, J., Kern, M., Pallandt, M., Schnur, R., ... & Zaehle, S. (2019). A new model of the coupled carbon, nitrogen, and phosphorus cycles in the terrestrial biosphere (QUINCY v1. 0; revision 1996). Geoscientific Model Development, 12(11), 4781–4802.
Vinh, T. V., Allenbach, M., Joanne, A., & Marchand, C. (2019). Seasonal variability of CO 2 fluxes at different interfaces and vertical CO 2 concentration profiles within a *Rhizophora* mangrove forest (Can Gio, Viet Nam). Atmospheric Environment, 201, 301–309.
West, G. B., Enquist, B. J., and Brown, J. H. (2009). A general quantitative theory of forest structure and dynamics. Proc. Natl. Acad. Sci. U.S.A. 106, 7040–7045.
Xu, X., Medvigy, D., Powers, J. S., Becknell, J. M., & Guan, K. (2016). Diversity in plant hydraulic traits explains seasonal and inter‐annual variations of vegetation dynamics in seasonally dry tropical forests. New Phytologist, 212(1), 80–95.
Yoshikai, M., Nakamura, T., Suwa, R., Argamosa, R., Okamoto, T., Rollon, R., ... & Nadaoka, K. (2021). Scaling relations and substrate conditions controlling the complexity of *Rhizophora* prop root system. Estuarine, Coastal and Shelf Science, 248, 107014.